**Proceedings of 32nd International Conference on Offshore Mechanics and Arctic Engineering**
**OMAE'13**
**June 9-14, 2013, Nantes, France**

# OMAE2013-10690

# NUMERICAL STUDY OF PARAMETRIC ROLL ON A FISHING VESSEL

**Marilena Greco**
NTNU/CeSOS/AMOS, Trondheim, Norway
CNR-INSEAN, The Italian Model Basin, Rome, Italy
Email: marilena.greco@ntnu.no;marilena.greco@cnr.it

**Claudio Lugni**
CNR-INSEAN, The Italian Ship Model Basin, Rome, Italy
CeSOS/AMOS, Trondheim, Norway
Email: claudio.lugni@cnr.it

## ABSTRACT

*Present research activity examines numerically the occurrence of parametric roll on a fishing vessel interacting with regular head-sea waves. The adopted solver is an efficient 3-D numerical Domain-Decomposition strategy for the seakeeping of a 6-dof vessel without and with small forward speed and possibly subjected to bottom-slamming and water-on-deck events. Here, the vessel has been assumed at rest and the excitation frequency is varied in the first parametric resonance zone and occurrence and features of the instability are examined in terms of nonlinearities of the incident waves and roll natural-to-incident wave frequency ratio. The analysis is performed both fully within the potential-flow theory and examining the effect on the parametric resonance of the viscous correction to the roll damping obtained from free-decay 3D model tests on the same ship. A system of four cables, horizontal in the mean configuration, will be used experimentally to limit the horizontal vessel motions. Here the numerical solver is used to analyze the influence of cable stiffness and of cable configuration on the vessel behavior and to help the design of the physical set up. The vessel has deep draft and high mean freeboard, these aspects work against the occurrence of bottom slamming and water-on-deck events. Without forward speed, no bottom slamming phenomena were observed while limited number of water-on-deck events with small amount of shipped liquid was recorded for the highest-frequency incident waves with largest steepnesses, among those causing parametric roll.*

## INTRODUCTION

Parametric roll involves resonant roll motion with instability behavior which may result in significant amplification of the roll motion (see *e.g.* [1]). The occurrence is connected with the time variation of the stability properties of the vessel due to changes in the restoring moment, and so of the transverse metacentric height $GM$, caused by high enough heave and pitch motions, as well as interaction with incident waves. The phenomenon is supported by large vertical ship motions, incident waves sufficiently aligned with the vessel longitudinal axis and not changing much in time in terms of period and amplitude. Another important factor is the roll damping, the lower it is the higher the possibility to have parametric roll will be. Finally there are ratios between the roll natural frequency and the excitation frequency, say $\omega_{4n}/\omega_e$, for which the instability occurs more easily. Considering an uncoupled Mathieu-type instability analysis for the roll motion, this gives $\omega_{4n}/\omega_e = 0.5$,1, 1.5, and so on, as more dangerous frequency ratios. This phenomenon is important for large vessels like container ships, as well as for small fishing vessels. In the former case the main issue is damage and loss of containers and cargo, while in the latter case the risk of capsizing is critical.

Here the case of a fishing vessel is analyzed numerically to identify the relevant physical and geometrical parameters involved and also to help the design of 3D model tests to analyze the phenomenon for a vessel free to oscillate in heave, pitch and roll, and able to oscillate also in other degrees of freedom, *e.g.* in surge, through the use of a cable system. Since almost regular incident waves propagating along the ship longitudinal axis are more of concern, the case of head-sea regular waves is investigated. In the next section the used numerical solver is briefly

described, then the experimental set-up is outlined and a physical investigation is carried out. In the last section main results are summarized and next research steps are indicated.

## THE NUMERICAL SOLVER

The problem of a rigid fishing vessel able to oscillate in its six degrees of freedom and to move forward with small speed in waves is solved using an efficient and accurate 3-D Domain-Decomposition (DD) strategy. The solver couples a 3D seakeeping potential-flow solver, with a bottom-slamming and a water-on-deck modeling. The bottom slamming is handled through a local Wagner-type [2] solution and using an improved occurrence criterion which combines the Ochi's velocity criterion with a pressure condition, [3]. The water shipping is solved assuming that only dam-breaking type of water on deck can occur. This is not a stringent condition because the most common water-on-deck scenario starts locally as a plunging wave hitting the ship deck near the front bow and has globally the features of a dam-breaking type event (see *e.g.* [4]). This means that the evolution of the shipped water can be studied within the shallow-water approximation. The problem is solved on a Cartesian grid fixed to the deck, using a splitting method to transform a 2D problem in the deck plane into a sequence of 1D coupled problems along the main axes of the computational grid. The problem equations are solved using an exact Riemann solver for the variables fluxes and stepping forward in time with a first order scheme. The boundary conditions along the deck and possibles superstructures are enforced using the level-set technique in [5]. The global wave-ship interaction solver assumes that incident waves and body motions are large relative to the scattering and radiation effects and so applies the weak-scatterer hypothesis (see e.g. [6]). This means the results are theoretically valid for wavelength-to-ship length ratio sufficiently large. Within this solution strategy, the impermeability body-boundary condition is satisfied averagely along the instantaneous wetted hull surface defined by the incident waves and the body motions. This leads to a correction of the scattering and radiation loads obtained from linear theory. Further, nonlinearities are retained up to the second order for Froude-Krylov and hydrostatic loads. Because the problem involves nonlinear loads and anyway the transient phase must be investigated to detect parametric roll excitation, the equations of motions are solved in time domain using the approach in [7]. The rigid-body motion equations are written along a body-fixed coordinate system with origin in the center of gravity and read

$$M\ddot{\xi} + \Omega \times M\dot{\xi} + A_\infty \dot{\beta} + \int_0^t K(t-\tau)\beta(\tau)\,d\tau = F_{0\,\mathrm{nlin}} + F_{h\,\mathrm{nlin}} + F_{\mathrm{wod}} + F_{\mathrm{slam}}\,. \quad (1)$$

Here, $M$ is the ship generalized mass matrix, $\xi \equiv (\xi_1,..,\xi_6)$ are the six rigid degrees of freedom, $\Omega$ is the angular velocity vector $(\dot{\xi}_4,\dot{\xi}_5,\dot{\xi}_6)$ and the upper dots indicate time ($t$) derivatives performed along the instantaneous body axes, *i.e* without accounting for the axes rotation. In equation (1), the cross product gives a six-component vector whose first three components are obtained by the cross-product of $\Omega$ with the first three components of $M\dot{\xi}$ and the remaining ones by the cross-product of $\Omega$ with the second three components of $M\dot{\xi}$. Further, $A_\infty$ is the infinite-frequency added-mass matrix and $K$ is the retardation function matrix. This equation system should be valid formally for linear problems in time domain but corrections due to nonlinear loads are included in the Froude-Krylov and hydrostatic loads, respectively, $F_{0\,\mathrm{nlin}}$ and $F_{h\,\mathrm{nlin}}$, and in the slamming and water-on-deck loads, respectively, $F_{\mathrm{slam}}$ and $F_{\mathrm{wod}}$, when such phenomena occur. A correction is also present in the added-mass and convolution-integral terms of equation (1). Indeed, within linear theory, $\beta$ is equal to $\dot{\xi}$ while here it is in general different and estimated in time from the body-boundary condition

$$V_n(x,t) = (V_{\mathrm{ship}} - V_{\mathrm{wave}}) \cdot n\,, \quad (2)$$

with $V_n$ the normal velocity at the wetted hull, $V_{\mathrm{ship}}$ the body velocity, $V_{\mathrm{wave}}$ the incoming-wave velocity, and $n$ the body normal vector. This implies that radiation and scattering phenomena are considered together. $V_n$ is expressed in terms of $N$ prescribed basis functions $\psi_i$,

$$V_n(x,t) = \textstyle\sum_{i=1}^{i=N} \beta_i(t)\psi_i(x)\,, \quad (3)$$

with $\beta_i$ the $i$-th component of $\beta$ and condition (2) is enforced through a Minimum Least-Square approach along the wetted hull defined by the incident waves and body motions. This provides the equations to find $\beta(t)$. The equations of motions are solved in time using a fourth-order Runge-Kutta scheme. When evolving from time $t$ to $t+\Delta t$ the water-on-deck and slamming loads, as well as the convolution integral terms, are estimated in $t$ and retained constant during the interval $\Delta t$, while the remaining loads are estimated at any time instant required by the scheme. Overall the solver is very efficient and can provide a time evolution of 400 periods in at most few hours on a modern pc. The most time consuming element is represented by the water-on-deck solution, this could be overcome in the future by parallelizing this part. The solver is described in detail in [3] and its different aspects have been verified and/or validated in *e.g.* [3], [8] and [9]. In particular, the parametric-roll predictions, without and with water-on-deck events, proved to be consistent with measurements in the case of a FPSO interacting with regular waves.

One must note that this compound solver estimates only the wave-radiation potential-flow roll damping. Viscous damping corrections can be modelled introducing empirical coefficients in the equation of motion.

**TABLE 1**. MAIN INFORMATION OF THE FISHING VESSEL AT MODEL SCALE.

| | |
|---|---|
| Length ($L$) | 2.95 m |
| Breadth ($B$) | 0.95 m |
| Draft ($D$) | 0.4 m |
| Displacement | 0.622 ton |
| Pitch Gyration radius | 0.28 $L$ |
| Roll Gyration radius | 0.38 $B$ |
| Metacentric height ($GM$) | 0.082 m |

## THE BASIC EXPERIMENTAL SET-UP

An experimental campaign on the parametric roll for a fishing vessel will be carried out at the CNR-INSEAN basin no.2, whose dimensions are: length x width x depth = 220 x 9 x 3.6 m. The main dimensions of the ship are given in table 1 and its 3D view is provided in the left of figure 1. This corresponds to a factor scale of 1:10. The model will be studied with a set of four cables arranged symmetrically with respect to the longitudinal ship axis (V-shaped configuration) as sketched in the right of figure 1. The cables will be not pre-tensioned; the effect of a pre-tension on the stiffness provided to the different motions might be relevant and will be examined in the future. As basic choice

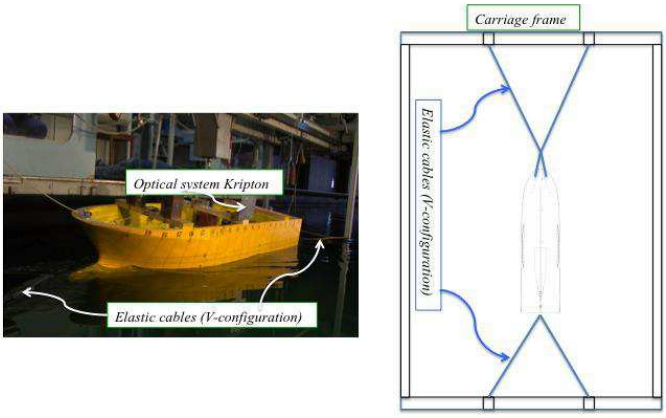


**FIGURE 1**. LEFT: 3D VIEW OF THE SHIP MODEL. RIGHT: SKETCH OF THE EXPERIMENTAL SET-UP TO BE USED IN PARAMETRIC-ROLL STUDIES.

the forward and aft cables are long, respectively, $L_{0cf} = 0.476L$ and $L_{0ca} = 0.433L$, with $L$ the ship length. The cable stiffnesses are given by $K_{cable} = AE/L_{0c}$ with $AE \simeq 392.61$Nm the product between the sectional area and the Young modulus of the cables. With the aim to investigate the influence of the cables on the occurrence of the parametric roll, the set-up is studied numerically in the present work.

At the moment, an intense experimental campaign in calm water has been performed to study the roll decay and the influence of the several appendages (bilge keels, skeg, propeller, rudder) that will be used in the final configuration for the future experiments in waves. Here, the free-decay tests in bare hull condition are used. To limit wall effects on the roll damping, dampers were introduced at the side walls of the model basin. Figure 2 shows the roll time history for the free decay test at zero forward speed and indicates a natural period $T_{4n} \simeq 2.74$ s; this is quite close to the roll natural period obtained from the numerical method, $T_{4n} \simeq 2.70$ s. One must note that this is the calm-water

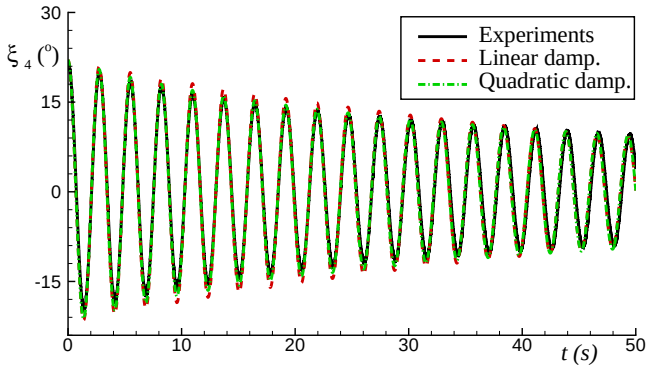


**FIGURE 2**. FREE DECAY IN ROLL FROM EXPERIMENTS AND NUMERICALLY USING LINEAR OR QUADRATIC DAMPING IDENTIFIED FROM THE MODEL TESTS.

1-dof roll natural period. In general, changes can be caused by the coupling with other ship degrees of freedom, as well as by incident waves that can modify the roll restoring moment. Assuming a 1-dof roll motion equation of the form

$$\ddot{\xi}_4 + p_1\dot{\xi}_4 + p_2\dot{\xi}_4|\dot{\xi}_4| + p_3\xi_4 = 0 \qquad (4)$$

with $p_1 = B_{44,1}/(I_{44}+A_{44})$, $p_2 = B_{44,2}/(I_{44}+A_{44})$ and $p_3 = C_{44}/(I_{44}+A_{44})$ and following the procedure in [10], the linear and quadratic approximations of the experimental roll damping have been obtained and are reported in table 2. Their correctness is verified by solving numerically equation (4) with initial roll amplitude from the model tests and comparing against the experimental decay (see figure 2). From the results, the quadratic damping follows slightly better the physical behavior while the linear damping underpredicts the roll decay at large roll amplitudes.

These coefficients will be introduced in the numerical solver to check the importance of viscous damping for the parametric roll.

**TABLE 2**. LINEAR AND QUADRATIC DAMPING FROM FREE-DECAY TESTS IN ROLL.

| Linear damp. | Quadratic damp. | |
|---|---|---|
| $p_1$ | $p_1$ | $p_2$ |
| 0.03575 | -0.0006 | +0.0734 |

## PHYSICAL INVESTIGATION

The incident-wave frequency was varied in the zone of the first fundamental resonance and the parametric roll was examined by varying the steepness $kA$ between 0.1 and 0.25 and performing simulations long $400T$, with $T$ the examined incident-wave period.

**No viscous damping correction and no cables** As first step, the vessel was studied at rest without viscous damping and without cables, so it was assumed free to oscillate in heave, pitch and roll, while interacting with head-sea regular waves. Table 3 examines the numerical occurrence of parametric roll in terms of incident-wave steepness $kA$ and of the calm-water 1-dof roll natural frequency-to-incident wave frequency, $\omega_{4n}/\omega$. Here $\omega_{4n}$ is

**TABLE 3**. NUMERICAL OCCURRENCE OF PARAMETRIC-ROLL RESONANCE.

| | $\omega_{4n}/\omega$ | | | | | |
|---|---|---|---|---|---|---|
| $kA$ | 0.46 | 0.47 | 0.48 | 0.49 | 0.50 | 0.51 |
| 0.10 | NO | NO | NO | YES | YES | NO |
| 0.15 | NO | NO | YES | YES | YES | NO |
| 0.20 | NO | YES | YES | YES | YES | NO |
| 0.25 | NO | YES | YES | YES | NO | NO |

taken as a reference since for the multi-dof ship the roll natural period is in general different than for a 1-dof system. From the results, nonlinearities are able to maintain or to bring the roll in the instability region for $\omega_{4n}/\omega$, lower than 0.5; at $\omega_{4n}/\omega = 0.5$ we have the opposite trend and at higher values of $\omega_{4n}/\omega$ no parametric roll is recorded. To examine this, let us take the 1-dof Mathieu-type stability analysis from which instability occurs more easily for frequency ratio equal to or near 0.5. With this in mind, the results can be explained by the fact that the nonlinearities tend to increase the roll natural frequency. So, if $\omega_{4n}/\omega$ is smaller than 0.5, the actual frequency ratio will be increased toward 0.5 and this might bring into the instability area by the nonlinearities. If $\omega_{4n}/\omega$ is equal or larger than 0.5, the actual frequency ratio will be increased to larger values and this might bring outside the instability area. As a confirmation of this, for each of the cases with instability occurrence, in steady-state conditions the roll oscillates with a frequency equal to twice the excitation frequency, *i.e.* the roll frequency is higher than the calm-water 1-dof natural frequency $\omega_{4n}$.

The case with $\omega_{4n}/\omega = 0.49$ is associated with instability at all examined $kA$, so it is used next for further investigation of the phenomenon. In particular, figure 3 gives the time history of the roll for the different steepnesses and highlights that a higher $kA$ leads to an earlier excitation of the instability, a shorter transient phase and a lower steady-state roll amplitude. The reasons be-

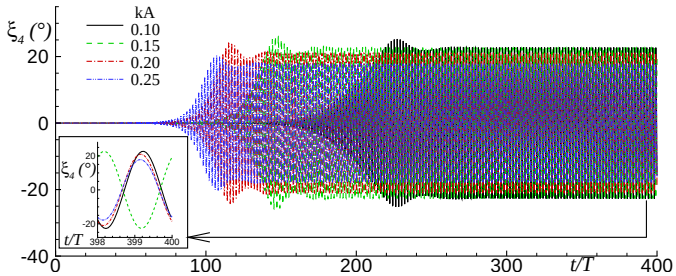


**FIGURE 3**. TIME HISTORY OF ROLL FOR $\omega_{4n}/\omega = 0.49$, WITHOUT DAMPING CORRECTION AND NO CABLES.

hind these features and the possible causes of parametric roll excitation are investigated in figure 4 using $kA = 0.1$ and 0.25. On the top, the time interval during the transient development of roll instability is shown for the two cases. The incident-wave eleva-

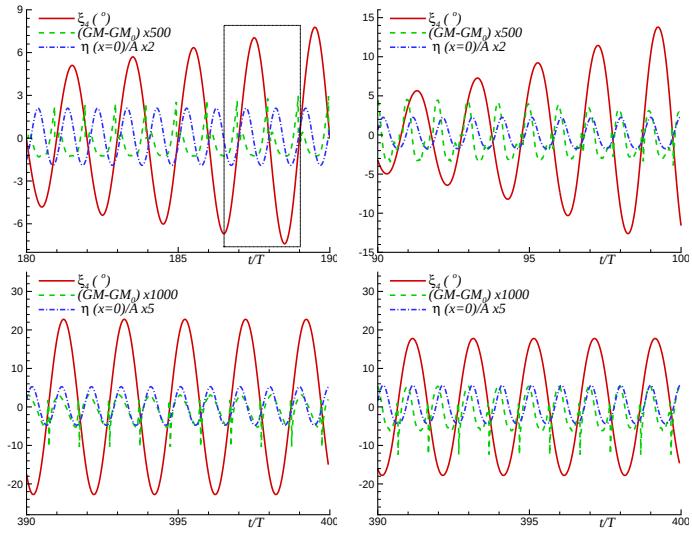


**FIGURE 4**. TRANSIENT AND STEADY-STATE PHASES DURING PARAMETRIC ROLL FOR THE CASE WITH $\omega_{4n}/\omega = 0.49$ AND WITH $ka = 0.1$ (LEFT) AND $kA = 0.25$ (RIGHT), WITHOUT DAMPING CORRECTION AND NO CABLES.

tion $\eta$ at the vessel center and the transverse metacentric height

*GM* are also given to help the discussion. Here *GM* is roughly obtained as $-F_{4h\,\mathrm{nlin}}/(\rho g \nabla \xi_4)$, with $\rho$ the water density, $g$ the gravity acceleration and $\nabla$ the ship displacement. The jumps observed in the figure are due to singularities for $\xi_4 = 0$, they have been reduced setting a threshold limit $\xi_4 = 1^\circ$ below which *GM* is set equal to the calm-water metacentric height $GM_0$. Let us focus on the time interval bounded by the dotted box for $kA = 0.1$, the incident-wave frequency is twice the roll natural frequency and the phasing between $\eta$ and the roll is so that a wave crest occurs mid-ship when $\xi_4$ is increasing. This means a reduction in time of the ship stability (and so of *GM* relative to $GM_0$) and the roll can reach larger amplitude than in the previous cycle. The wave trough occurs mid-ship when the roll is decreasing, this makes faster the decrease of the motion and the later occurrence of a new wave crest supports again a roll rise in the opposite ship side (negative roll). This phenomenon is similar for the two *kA* cases but the steeper waves lead to a larger *GM* variation relative to the calm-water value, in particular to larger periodic reductions, and this allows a much faster rise of the roll amplitude. In this example, within a time interval of $2T$, the case with $kA = 0.1$ leads to an increase in the roll amplitude $\xi_{4a}$ less than 3 degrees while $kA = 0.25$ is associated with an increase more than twice this value. Bottom plots of the figure consider the same cases but when steady-state conditions are reached. The relative phase between $\xi_4$ and $\eta$ is the same as in the transient phase discussed above while *GM* is changed. In particular *GM* is almost in phase with the incident-wave elevation mid-ship and this enable steady state conditions. Indeed, when a wave crest occurs which would tend to reduce the waterplane area and so the stability, then *GM* has also a large value, probably due to coupling of roll with heave and pitch motions, and this works against the increase of the roll amplitude in time. From the results, $kA = 0.1$ is associated with larger steady-state amplitude of roll.

The possible reason why the higher the steepness the lower the steady-state wave amplitude could be found in the coupling with heave and pitch. This is investigated in figure 5 for the same cases. For the lower steepness (left plots), during the transient phase (top plot), the roll extremes (maxima and minima) occur at the maximum pitch (positive with bow downward) and at the minimum heave (positive upward). This means that when the roll increases in magnitude (at any vessel side) the ship is lifted up and pitches bow down. This supports the roll increase. As the roll amplitude increases, the nonlinear effects connected with the large motions slightly modify the roll oscillation period and cause an increasing phase shift between $\xi_4$ and the other degrees of freedom during the transient. This leads to a final steady-state phase link (bottom plot) where when the roll increases in magnitude the heave and pitch are almost zero so that there is no support to increase the roll amplitude in time from the heave and pitch motions. For the larger steepness (right plots), the nonlinearities become important earlier in time therefore also in the transient phase heave and pitch are almost zero when the roll increases in magnitude. This leads the steady-state conditions to be reached earlier and so with lower roll amplitude. One must note that also heave and pitch are affected by the occurrence of parametric roll, they increase in amplitude and their mean values are shifted when the roll amplitude is sufficiently large (compare top and bottom plots). In particular the instability tends to rise the hull and to pitch her more bow down. This is reasonable because large roll will increase the displaced volume mostly in the aft part of the ship (much wider than the bow part) so we can expect a buoyancy related to it pushing the bow down and the hull up.

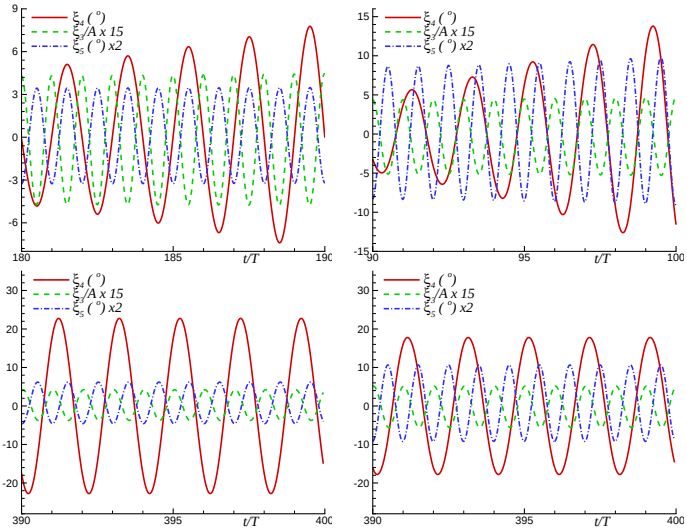


**FIGURE 5**. TRANSIENT AND STEADY-STATE PHASES DURING PARAMETRIC ROLL FOR THE CASE WITH $\omega_{4n}/\omega = 0.49$ AND WITH $ka = 0.1$ (TOP) AND $kA = 0.25$ (BOTTOM), WITHOUT DAMPING CORRECTION AND NO CABLES.

What discussed above is somehow summarized in figure 6 in terms of the righting arm *GZ* and the roll velocity as a function of the roll motion during the vessel evolution. From the results, the case with higher *kA* leads to a larger variation of the *GZ* slope (see enlarged view in the left plot), which is the same as *GM* for small $\xi_4$, and to a quicker rise of the roll velocity in time (see right plot). However the steady state roll amplitude is more limited as indicated by the arrows giving the radii of the zones with largest concentration of curves in the $(\xi_4, \dot{\xi}_4)$ plane for each case. In both *kA* cases the *GZ* curve is increasing with the roll which suggests that there is not danger for vessel capsizing in these conditions.

The effects of *kA* are globally the same for all incident-wave frequencies. This is summarized by figure 7 in terms of the time required to reach the first peak in the roll envelope, $t_{max}$, corresponding to the largest roll value, and in terms of the steady-state roll amplitude, $\xi_{4a}$. An exception for the time trend is represented by the case with $\omega_{4n}/\omega = 0.5$ and $kA = 0.20$. $t_{max}$ seems

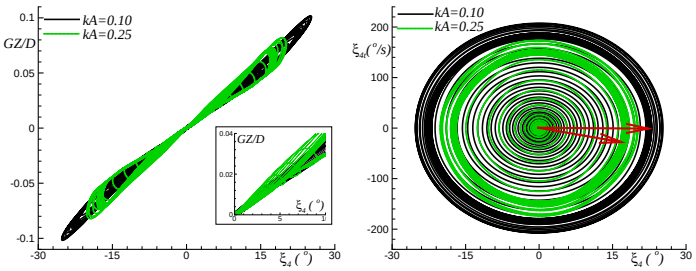


**FIGURE 6**. *GZ* AND ROLL VELOCITY $\dot{\xi}_4 = \xi_{4t}$ AS FUNCTIONS OF THE ROLL FOR CASE WITH $\omega_{4n}/\omega = 0.49$, WITHOUT DAMPING CORRECTION AND NO CABLES. HERE $D$ IS THE VESSEL DRAFT.

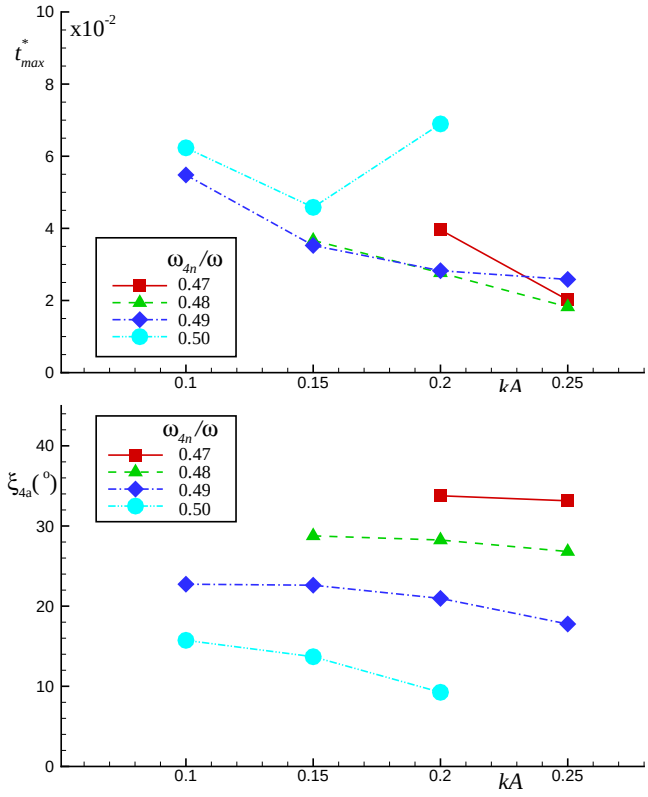


**FIGURE 7**. TIME REQUIRED TO REACH THE FIRST ROLL PEAK (TOP) AND STEADY-STATE ROLL AMPLITUDE AS FUNCTIONS OF $kA$ AND INCIDENT WAVE-TO-NATURAL ROLL FREQUENCY RATIO, WITHOUT DAMPING CORRECTION AND NO CABLES. $t^*_{max} = t_{max}\sqrt{g/L}$.

to be more affected by $kA$ than by $\omega_{4n}/\omega$ while the opposite is documented by the steady-state amplitude which increases almost linearly as $\omega_{4n}/\omega$ decreases.

Because of the deep draft and of the high mean freeboard the vessel is not sensitive to bottom-slamming and water-on-deck phenomena, at least without forward speed. Present investigations document no bottom slamming and limited number of water shipping for $\omega_{4n}/\omega = 0.47$ with $kA = 0.20$ and $kA = 0.25$. The events occurred when the roll reached the largest value during the transient (the first peak discussed above) and were associated with very small amount of shipped liquid which was not relevant for the vessel behavior at sea.

**With viscous damping correction and no cables** The viscous damping corrections obtained from the experiments were introduced in the potential-flow solver to check the effects in the roll-instability occurrence and features. The damping did not change the occurrence of the phenomenon but affected transient phase and steady-state conditions depending on the choice between linear and quadratic damping corrections. This is discussed in figure 8 for the case with $\omega_{4n}/\omega = 0.49$ and $kA = 0.1$ as an example. From the results, the quadratic damping practically does not affect the duration of the transient phase while the linear damping causes a delay of the steady-state conditions of several incident-wave periods. This could be due to the fact that the liner damping is more effective than the quadratic damping (whose linear contribution is almost zero, see table 2) at lower roll amplitudes. As expected, the steady-state amplitudes with viscous damping correction are slightly lower than without and the quadratic damping appears slightly more effective than the linear correction. This is reasonable because the quadratic damping has a term proportional to the square of the roll velocity, and so to the square of the roll amplitude. Another difference between the two damping corrections in terms of effectiveness comes from the roll natural frequency. The larger $\omega_{4n}$ the more effective the quadratic damping correction is expected to be. The effects of linear and quadratic viscous damping corrections for all cases with parametric roll are examined in figures 9 and 10, respectively. In figure 9 the results for case with $\omega_{4n}/\omega = 0.5$ and $kA = 0.20$ are not reported, though there is parametric roll. This is because the linear damping has made so slow the instability process that steady-state conditions are not reached within a $400T$ evolution. From the results the influence of $kA$ and $\omega_{4n}/\omega$ remains qualita-

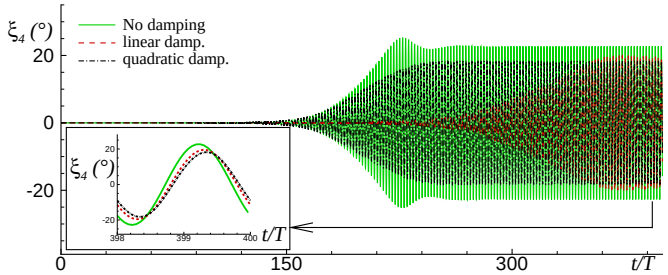


**FIGURE 8**. TIME HISTORY OF ROLL FOR $\omega_{4n}/\omega = 0.49$ AND $kA = 0.1$. NO CABLES.

tively the same with the viscous damping. The linear damping is more effective at lower excitation frequencies, *i.e.* higher $\omega_{4n}/\omega$, in enlarging $t_{max}$, while the quadratic term in general does not affect much the transient duration. Both damping corrections tend to slightly reduce the steady-state roll amplitude, especially at the lowest $kA$.

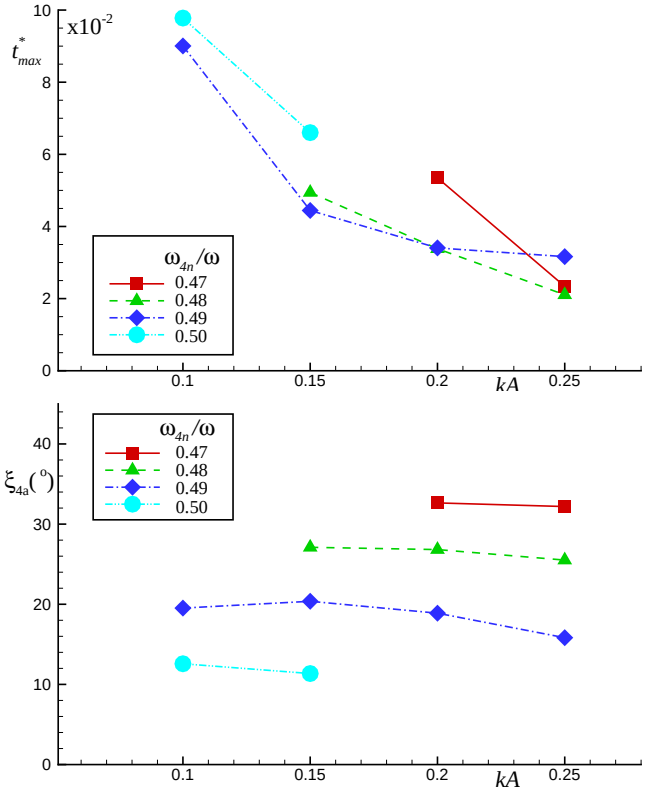


**FIGURE 9**. TIME REQUIRED TO REACH THE FIRST ROLL PEAK (TOP) AND STEADY-STATE ROLL AMPLITUDE AS FUNCTIONS OF $kA$ AND INCIDENT WAVE-TO-NATURAL ROLL FREQUENCY RATIO, WITH LINEAR VISCOUS DAMPING CORRECTION AND NO CABLES. $t^*_{max} = t_{max}\sqrt{g/L}$.

**With surge due to cables** The effect of cables was examined by allowing also surge motion of the vessel, while yaw and sway are restrained. The yaw influence can be large and will be investigated in detail as a next step. For simplicity the sway is not examined but it can also matter and should be considered for a more realistic scenario in the future.

The physical cables have been modelled in the solver assuming fixed the four nodes farthest from the vessel and free to move rigidly with the vessel the remaining two nodes. The loads acting on the vessel due to the cables were modelled as restoring forces applied at the free nodes and directed along each cable when the

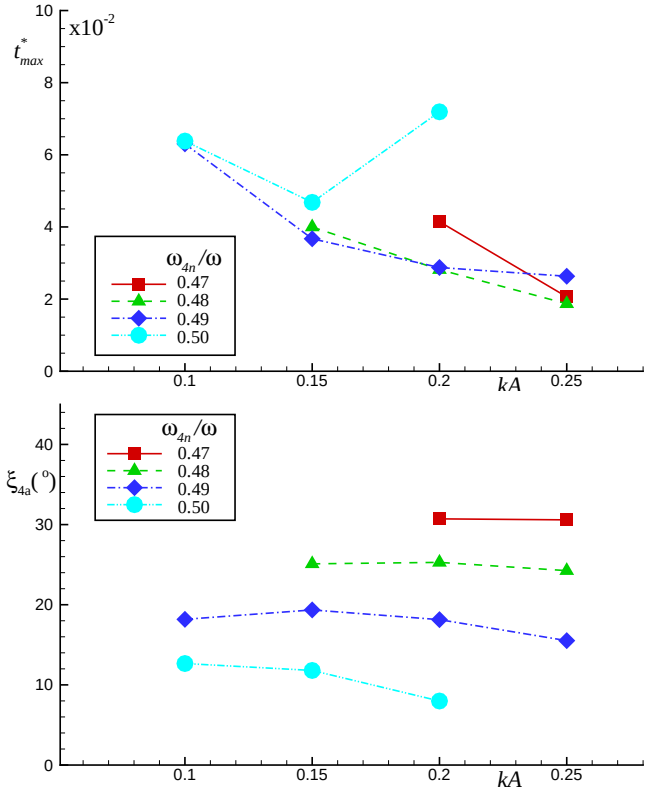


**FIGURE 10**. TIME REQUIRED TO REACH THE FIRST ROLL PEAK (TOP) AND STEADY-STATE ROLL AMPLITUDE AS FUNCTIONS OF $kA$ AND INCIDENT WAVE-TO-NATURAL ROLL FREQUENCY RATIO, WITH QUADRATIC VISCOUS DAMPING CORRECTION AND NO CABLES. $t^*_{max} = t_{max}\sqrt{g/L}$.

cable is in tension. If the system remains symmetric about the longitudinal axis, the cable force system will not give any lateral component. When roll is excited, the cables will result in forces in all three directions affecting the translational motions, their torques will influence the rotational motions.

The stiffness of the cables leads to a surge natural period $T_{1n} \simeq 7.71$s which is about three times the roll natural period. Due to the head-sea conditions, usually the surge motion has also a drift toward the ship stern and the amount depends on the stiffness of the cables, the higher the stiffness the lower the drift is. The presence of the surge does not modify the occurrence plane of the roll instability and affects in a limited way the features of the parametric roll, as documented by figure 11. The surge affects mostly the cases with higher steepnesses because in those cases the surge motion has larger oscillation amplitudes and can affect more the other motions and so the roll. In terms of steady-state amplitude, the effect is practically negligible, while the surge can both delay and accelerate the instability. This depends on the phasing between the different loads on the vessel. For instance, if the surge motion is large then the center of the

ship will experience rather different Froude-Krylov loads, further the occurrence in time of a wave crest or trough mid-ship will be also affected. One must remember that it is important to

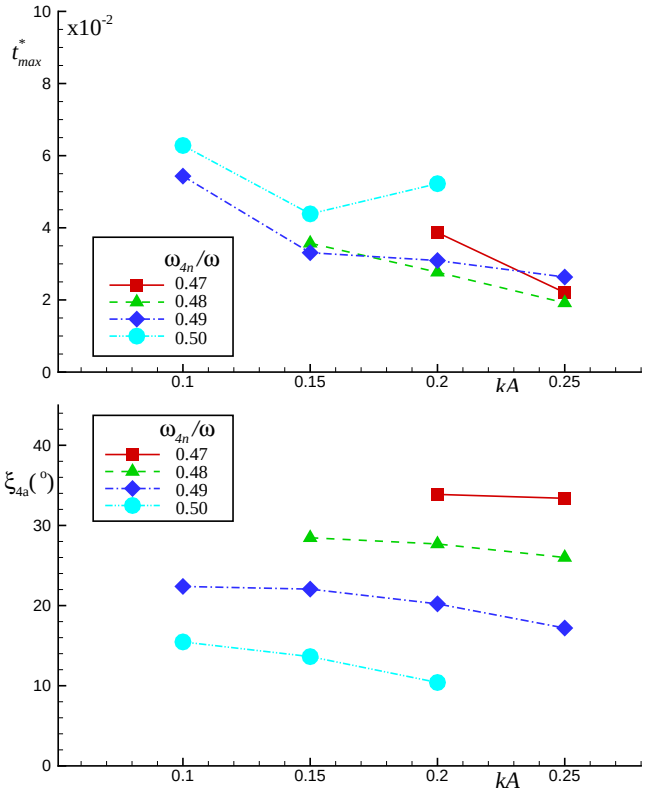


**FIGURE 11**. TIME REQUIRED TO REACH THE FIRST ROLL PEAK (TOP) AND STEADY-STATE ROLL AMPLITUDE AS FUNCTIONS OF $kA$ AND INCIDENT WAVE-TO-NATURAL ROLL FREQUENCY RATIO, WITHOUT DAMPING CORRECTION AND WITH SURGE DUE TO CABLES. $t^*_{max} = t_{max}\sqrt{g/L}$.

have a stiffness sufficiently small so to have a fictitious surge natural period that does not change the physical problem examined. On the other hand the stiffness can not be too small. With the basic stiffness considered, the case with highest incident-wave frequency documented an envelope in the roll motion connected with the surge natural period. This is shown in figure 12 for $kA = 0.25$. The roll motion (top plot) without viscous damping clearly shows this envelope connected with the surge natural period (bottom plot). Probably this is because the incident-wave period is much different from the surge natural period and the surge oscillations are large enough to modify extreme values of hydrostatic and Froude-Krylov roll moments. Using linear and quadratic viscous damping, the envelope disappears as the surge oscillations around the mean drift become very limited. Here also the viscous damping in surge due to the presence of the cables has been included and estimated experimentally using surge free-decay tests, similarly as done for the roll. If the cable stiff-

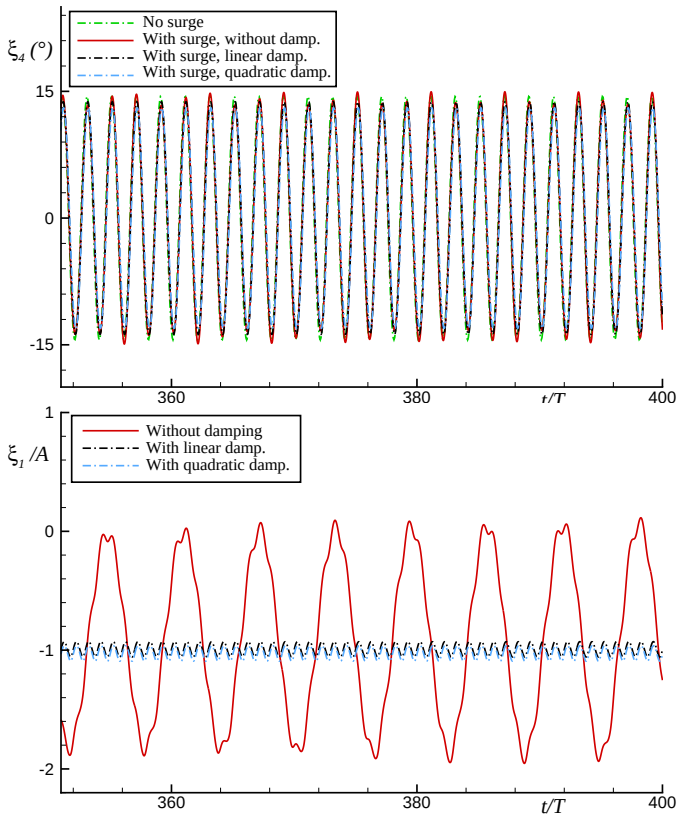


**FIGURE 12**. TIME HISTORY OF ROLL (TOP) AND SURGE (BOTTOM) FOR THE CASE WITH $\omega_{4n}/\omega = 0.47$ AND $kA = 0.25$.

ness is halved the roll behavior becomes less regular and quite affected by the surge motion because of the much larger surge oscillation amplitude (see figure 13).

Another important issue is the sensitivity of the parametric roll to the cable configuration. This is examined in table 4 in terms of $t_{max}$ and steady-state roll amplitude $\xi_{4a}$ using again the case $\omega_{4n}/\omega = 0.49$ with $kA = 0.1$ and 0.25 as an example. No viscous damping correction is considered. The vertical position of the cable nodes has been shifted from $z = 0$ to $z = \pm z_G$, with $z_G$ the coordinate of the center of gravity and the fixed nodes have been moved apart or toward the vessel along the longitudinal axis of a quantity $\Delta x = \pm 0.1 L_{0c}$, with $L_{0c}$ the basic length of the examined cable. The first variation is relevant for the moments induced by the cables, while the second one corresponds to a change in the cable length and so in the cable stiffness. The longer the cable the lower its stiffness is. From the results, these variations do not cause any relevant change in terms of parametric roll, so the sensitivity to the cable set-up does not appear

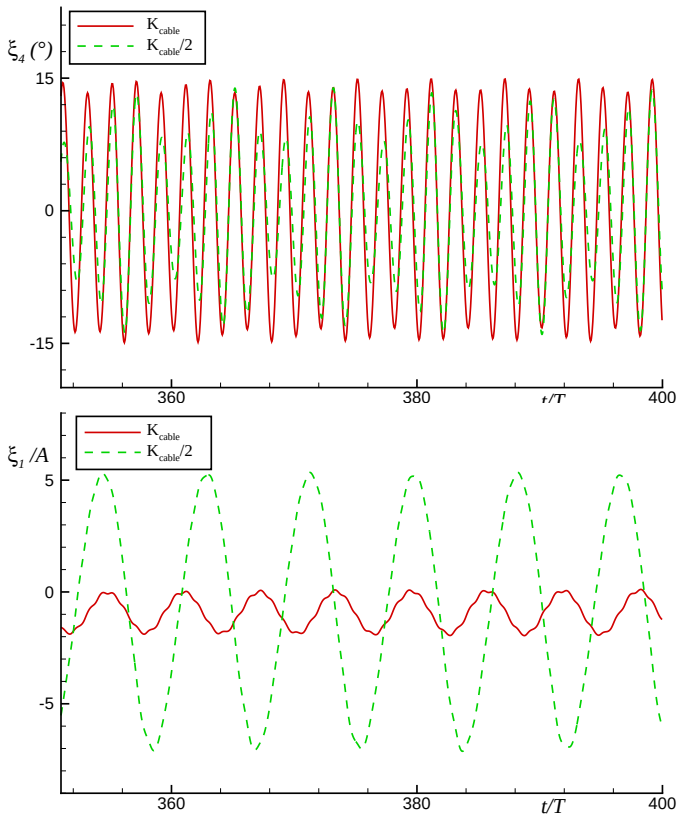


**FIGURE 13**. TIME HISTORY OF ROLL (TOP) AND SURGE (BOTTOM) FOR THE CASE WITH $\omega_{4n}/\omega = 0.47$ AND $kA = 0.25$. $K_{cable}$ IS THE STIFFNESS OF EXPERIMENTAL CABLES.

**TABLE 4**. EFFECTS OF CABLE CONFIGURATION ON $t^*_{max} = t_{max}\sqrt{g/L}$ AND ON THE STEADY-STATE $\xi_{4a}$ (IN DEGREES) FOR CASE $\omega_{4n}/\omega = 0.49$ WITH $kA = 0.1$ (=1) AND $kA = 0.25$ (=2).

| | $z, \Delta x = 0$ | $z = -z_G$ | $z = +z_G$ | $\Delta x = -0.1L_{0c}$ | $\Delta x = +0.1L_{0c}$ |
|---|---|---|---|---|---|
| 1: $t^*_{max}$ | 173.45 | 170.38 | 173.46 | 173.44 | 173.45 |
| 2: $t^*_{max}$ | 84.10 | 85.63 | 85.63 | 84.09 | 85.63 |
| 1: $\xi_{4a}$ | 22.39 | 22.39 | 22.30 | 22.43 | 22.40 |
| 2: $\xi_{4a}$ | 17.20 | 17.20 | 17.10 | 17.28 | 17.14 |

high.

## SUMMARY AND FUTURE STEPS

The occurrence and features of parametric roll were examined for a small fishing vessel at rest in regular head-sea conditions. The effects of the incident-wave frequency and steepness, of the viscous damping and of the cable stiffness and configuration to be used experimentally for a physical study of the problem, were examined. Globally, the higher $kA$ the faster the instability occurrence and the smaller the steady-state roll amplitude are. The latter is more sensitive to $\omega_{4n}/\omega$ and increases almost linearly as this ratio decreases. Higher incident-wave nonlinearities help triggering parametric roll for $\omega_{4n}/\omega < 0.5$ while they avoid the instability for $\omega_{4n}/\omega = 0.5$. A linear viscous damping delays much the parametric-roll occurrence while a quadratic damping does not affect the transient. One should consider an equivalent linear viscous damping instead of the linear damping defined here to check the sensitivity of $t_{max}$ to this parameter. The steady-state roll amplitude is slightly reduced by the damping. The surge due to the cables does not affect much the parametric roll features for the chosen cable stiffness. The latter is an important parameter and should be properly tuned to avoid a behavior of the vessel different than in open sea when using model tests.

The next step will be to examine the yaw motion which could lead to an additional instability phenomenon when couples with roll, depending on the cable features. We will then examine the effect of small forward speed for the parametric roll. In this case we can have both a direct and an indirect influence. In fact, the forward speed causes among the others a different excitation frequency experienced by the vessel and so it leads to a different frequency range where the parametric roll is experienced. Moreover, it can cause more easily water on deck depending on the vessel conditions. Sufficiently heavy water shipping may affect and be affected by parametric roll, as examined for instance in [9].

## ACKNOWLEDGMENT

This research activity is partially funded by the Centres of Excellence CeSOS and AMOS, NTNU, Norway, partially by Norwegian Research Council within the Research Project 'Numerical Simulation of Complex System' and partially by the Flagship Project RITMARE - The Italian Research for the Sea - coordinated by the Italian National Research Council and funded by the Italian Ministry of Education, University and Research within the National Research Program 2011-2013.

## REFERENCES

[1] Faltinsen, O. M., 2005. *Hydrodynamics of high-speed marine vehicles*. Cambridge University Press, Cambridge, UK.

[2] Wagner, H., 1932. "Uber stoss- und gleitvorgange an der oberflache von flussigkeiten". *ZAMM*, ***12***(4), pp. 192–235.

[3] Greco, M., and Lugni, C., 2012. "3-d seakeeping analysis with water on deck and slamming. part 1: numerical solver". *Journal of Fluids and Structures*, ***33***.

[4] Greco, M., Colicchio, G., and Faltinsen, O. M., 2007. "Shipping of water on a two-dimensional structure. part 2". *Journal of Fluid Mechanics*, ***581***, pp. 371–399.

[5] Colicchio, G., 2004. "Violent disturbance and fragmenta-

tion of free surfaces". PhD thesis, University of Southampton, Southampton, UK.
[6] Pawlowski, J., 1991. "A theoretical and numerical model of ship motions in heavy seas". In SNAME Transactions, Vol. 99, pp. 319–315.
[7] Cummins, W., 1962. "The impulse response function and ship motions". *Symposium on Ship Theory, Schiffstechnik,* ***9***, pp. 101–109.
[8] Greco, M., Bouscasse, B., and Lugni, C., 2012. "3-d seakeeping analysis with water on deck and slamming. part 2: Experiments and physical investigation". *Journal of Fluids and Structures*(33).
[9] Greco, M., and Lugni, C., 2012. "Numerical and experimental study of parametric roll with water on deck". In Proc. of Int. Conference on Violent Flows (VF-2012).
[10] Faltinsen, O. M., 1990. *Sea loads on ships and offshore structures*. Cambridge University Press, Cambridge, UK.